

Partially acrylated linseed oil UV-cured coating containing a dihemiacetal ester for the corrosion protection of an aluminium alloy

David Boucher, Vincent Ladmiral, Claire Negrell, Nicolas Caussé, Nadine Pébère

▶ **To cite this version:**

David Boucher, Vincent Ladmiral, Claire Negrell, Nicolas Caussé, Nadine Pébère. Partially acrylated linseed oil UV-cured coating containing a dihemiacetal ester for the corrosion protection of an aluminium alloy. Progress in Organic Coatings, 2021, 158, pp.106344. 10.1016/j.porgcoat.2021.106344 . hal-03320308

HAL Id: hal-03320308

https://hal.umontpellier.fr/hal-03320308

Submitted on 20 Oct 2021

HAL is a multi-disciplinary open access archive for the deposit and dissemination of scientific research documents, whether they are published or not. The documents may come from teaching and research institutions in France or abroad, or from public or private research centers.

L'archive ouverte pluridisciplinaire **HAL**, est destinée au dépôt et à la diffusion de documents scientifiques de niveau recherche, publiés ou non, émanant des établissements d'enseignement et de recherche français ou étrangers, des laboratoires publics ou privés.

OATAO
Open Archive Toulouse Archive Ouverte

Open Archive Toulouse Archive Ouverte (OATAO)

OATAO is an open access repository that collects the work of Toulouse researchers and makes it freely available over the web where possible

This is an author's version published in: http://oatao.univ-toulouse.fr/28411

Official URL: https://doi.org/10.1016/j.porgcoat.2021.106344

To cite this version:

Boucher, David and Ladmiral, Vincent and Negrell, Claire and Caussé, Nicolas and Pébère, Nadine *Partially acrylated linseed oil UV-cured coating containing a dihemiacetal ester for the corrosion protection of an aluminium alloy.* (2021) Progress in Organic Coatings, 158. 106344. ISSN 0300-9440

Any correspondence concerning this service should be sent to the repository administrator: tech-oatao@listes-diff.inp-toulouse.fr

Partially acrylated linseed oil UV-cured coating containing a dihemiacetal ester for the corrosion protection of an aluminium alloy

David Boucher [a,b], Vincent Ladmiral [a], Claire Negrell [a], Nicolas Caussé [b,*], Nadine Pébère [b]

[a] ICGM, Univ. Montpellier, ENSCM, CNRS, Montpellier, France
[b] CIRIMAT, ENSIACET, 4 allée Emile Monso, Toulouse, France

ARTICLE INFO

Keywords:
Bio-based coating
Barrier properties
Water uptake
Self-healing
Glass transition temperature
Electrochemical impedance spectroscopy

ABSTRACT

The present work focused on the development of a partially bio-based polymer matrix for the corrosion protection of the 3003 aluminium alloy. A dihemiacetal ester (1,10-dibutoxyethyl sebacate (DBES)) was added to the formulation to afford, after an additional thermal treatment, further cross-linking and a repairing effect of the polymer matrix. First, an epoxidized linseed oil was partially acrylated and subsequently copolymerized with (3,4-dihydroxyphenetyl)-acrylamide and *N*,*N*-dimethyl acrylamide, with and without DBES under UV irradiation. Under thermal treatment, the DBES released dicarboxylic acid able to react with epoxy functions. The corrosion protection of the resulting coatings (with and without DBES and with and without the thermal treatment) was assessed by electrochemical impedance spectroscopy (EIS). The diagrams were obtained for various immersion times in a 0.5 M NaCl solution. The coatings had good barrier properties, which remained stable throughout the duration of the impedance measurements (two weeks). The addition of the DBES in the formulation, followed by the thermal treatment, resulted in an increase of the barrier properties, a decrease of water uptake and a healing of some small matrix defects. The improvement of the anticorrosion ability of the coating containing the DBES after the thermal treament was attributed to an additional cross-linking. This work illustrates an original strategy for the development of self-healing bio-based coatings by using temporarily protected functions (here, dihemiacetal ester functions).

1. Introduction

Vegetable oil-based polymers are increasingly used to develop greener organic coatings for corrosion protection. Protective coatings from bio-based polyurethanes [1–5], polybenzoxazines [6–8], alkyd resins [9,10], epoxidized oils [11–14] or cardanol [15], and even chitosan [16] have been recently reported in the literature. Epoxidized oils are of particular interest. These oils can be obtained from a wide variety of vegetable sources. Depending on their origin, they generally possess a high functionality and are naturally highly hydrophobic due to their triglyceride structures [17].

The first attempt to use an epoxidized oil for the production of anticorrosive coatings has been reported by Thames and Yu in 1999 [18]. They used vernonia oil (VO) or epoxidized soybean oil (ESO) for the preparation of cationic UV-curable coatings on a steel substrate. From salt spray test, they concluded that the occurrence of surface blistering decreased when the oil (VO or ESO) content was increased in the coating. Ahmad et al. [19] have developed epoxy-amine coatings from epoxidized squamosa oil that showed acceptable corrosion protection of steel or aluminium alloy substrates in 10 wt.% NaOH, HCl or NH_4OH solutions, but lower protection in a 3.5 wt.% NaCl solution. More recently, interesting protective properties were shown with acrylated epoxidized oils matrices cured by thermal or UV radical polymerization [11–14].

These coatings from vegetable oils, in the absence of corrosion inhibitors or fillers, usually present lower protective performance compared to conventional materials affecting the long-term sustainability [12,20]. To improve the corrosion protection, these new protective systems must have both good barrier properties and good adhesion to the metal substrate. Adhesion is an important parameter for the metal/coating interface durability [21–23]. The acrylated epoxidized oils do not have intrinsic functions to interact with the metal substrate [13]. Thus, the addition or the copolymerization of a bio-based adhesion promoter into a coating is of interest. Catechol derivatives (naturally used by mussels to stick on rocks) have shown high adhesion on inorganic surfaces [24,25] and they can easily be acrylated or

* Corresponding author.
E-mail address: nicolas.causse@ensiacet.fr (N. Caussé).

https://doi.org/10.1016/j.porgcoat.2021.106344

methacrylated [26–28]. Acrylated or methacrylated catechol derivatives can afterwards be copolymerized with acrylated matrix [29] to improve its adhesion.

To extend the service life of these bio-based coatings, self-healing properties can be implemented [30,31]. One possibility is to add reactive species into the polymer matrix, which will react "on demand" to restore the barrier properties in case of defects [32]. The reactive species often need to be protected through storage in capsules or hollow fibers [33]. Despite their popularity, the use of containers has some drawbacks such as a decrease in the mechanical properties of the coating as well as a limitation in the amount of reactive species that can be introduced into the polymer matrix [34]. Thus, the protection of reactive functions by the use of thermally reversible chemical functions represents a valuable alternative to capsules or hollow fibers. Hemiacetal ester functions are known to thermally dissociate and release carboxylic acids and vinyl ethers between 100 and 250 °C, depending on their structures [35,36]. For automotive coil-coating applications, Yamamoto and Ishidoya [37] have converted carboxylic acids into hemiacetal ester by the reaction with alkyl vinyl ethers in order to improve storage stability of coatings. The blocked carboxylic acids prevented a premature reaction of the acids with epoxide. The hemiacetal ester compounds, stable under ambient conditions, can react on demand at elevated temperature to reform the original carboxylic acids. Kovash et al. [38] have converted solid diacids that are incompatible with epoxy matrices, into liquid dihemiacetal esters, easier to formulate for the preparation of fully bio-based thermosets. Komatsu et al. [39–42] have developed "on demand" a thermally cross-linkable polymer carrying hemiacetal ester functions as side chains which can react with epoxides. To the best of our knowledge, the use of hemiacetal ester functions for the self-healing of organic coatings for the corrosion protection has never been explored.

The present paper aims at developing and characterizing a partially bio-based protective coating prepared by polymerization under UV. It consisted of a partially acrylated epoxidized linseed oil, *N,N*-dimethyl acrylamide used as reactive diluent and (3,4-dihydroxyphenetyl) acrylamide as adhesion promoter. A dihemiacetal ester (1,10-dibutoxyethyl sebacate) was introduced into the coating to investigate its ability, when thermally treated, to improve the barrier properties of the coating and/or to self-heal the polymer matrix. Two coating systems (with and without the dihemiacetal ester) were applied onto the 3003 aluminium alloy (AA3003) and four coatings were compared (with and without the dihemiacetal ester and with and without a thermal treatment). The corrosion protection performance of the coatings was assessed by electrochemical impedance spectroscopy (EIS) during immersion in a 0.5 M NaCl solution [43,44]. The glass transition temperatures (T_g) of the different coatings (on free-standing films) were determined by differential scanning calorimetry (DSC).

2. Experimental

2.1. Materials

Dopamine hydrochloride, acryloyl chloride, acrylic acid, *N,N*-dimethyl acrylamide, butyl vinyl ether and sebacic acid were obtained from Sigma-Aldrich. N-dodecyl dihydrogen phosphate was purchased from abcr GmbH. Merginate Elo (epoxidized linseed oil) was kindly provided by Hobum Oleochemical GmbH. All reactants were used as received.

A 3003 aluminium alloy (AA3003) was used as metal substrate. Its chemical composition in weight percent was: Cu 0.05; Fe 0.7; Mn 1.5; Si 0.6; Zn 0.1 and Al to balance. The specimens consisted of 152 mm × 102 mm × 0.8 mm plates, purchased from Labomat. The samples surface were abraded using emery papers until 600 grade and then successively cleaned with acetone and ethanol.

2.2. Synthesis of the coating constituents

The epoxidized linseed oil was partially acrylated according to the following protocol [45]: 100 g of the epoxidized linseed oil with an epoxide equivalent weight (EEW) of 180 g/eq ($5.6\ 10^{-1}$ moles/eq) was mixed with 20 g ($2.8\ 10^{-1}$ mol) of acrylic acid, $2.2\ 10^{-1}$ g ($8.4\ 10^{-4}$ mol) of triphenylphosphine as catalyst and $6.6\ 10^{-2}$ g ($6.0\ 10^{-4}$ mol) of hydroquinone as polymerization inhibitor at 80 °C for 8 h in a round bottom flask wrapped in aluminium foil and equipped with a condenser. This mixture was then left at room temperature for 30 min before being solubilized in ethyl acetate. The organic phase was washed four times with a 10 wt.% NaOH solution to obtain a clear and colourless liquid which was then dried using $MgSO_4$. The solvent was evaporated in a brown glass container under vacuum at 50 °C for at least 24 h.

(3,4-Dihydroxyphenethyl)acrylamide (DHPA) (Fig. 1a), used as adhesion promoter, was synthesized (from dopamine hydrochloride and acryloyl chloride) based on a previously described procedure [27]. 1, 10-Dibutoxyethyl sebacate (DBES) (Fig. 1b) was prepared (from butyl vinyl ether and sebacic acid) according to a previously described protocol [46].

2.3. Coating samples

The coatings were prepared by first mixing DHPA with *N,N*-dimethyl acrylamide (DMA). Then, the partially acrylated epoxidized linseed oil (AELO) was added to this mixture. For the formulation containing the DBES, it was added at the same time as the AELO. The mixtures were deposited onto the AA3003 substrate using a baker applicator from Brant Industry (10 cm width and 150 μm in height). Both formulations (with and without DBES) were copolymerized using a Fusion UV LC6B Benchtop Conveyor. Six passages at a speed of 1 m/min were carried out. It should be emphasized the fact that no photoinitiator was used in the formulations. Several studies demonstrated that acrylated monomers can be photopolymerized by self-initiation [47,48].

For the thermal treatment, the samples were placed in an oven at 140 °C for 6 h. The choice of this temperature will be justified in Section 3.2. To determine the glass transition temperature of the coatings, free-standing films were also produced by using the same protocol but replacing the aluminium substrate by polytetrafluoroethylene sheets. Table 1 summarizes the composition, the average thickness as well as the acronyms of the four coatings (with or without DBES and with or without the thermal treatment). The coating thickness was measured by an ultrasonic probe. In Table 1, mean thickness values were determined from three samples and eight measurements at different locations on

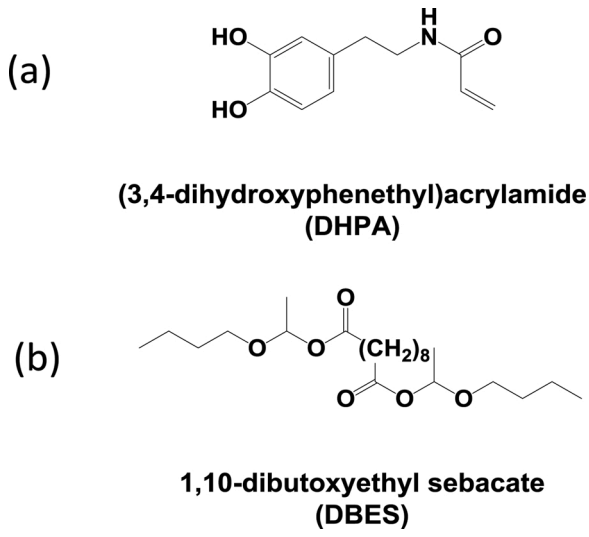


Fig. 1. Structure of: (a) DHPA and (b) DBES.

Table 1
Composition of the four coatings.

	DBES-free coating (CF)	DBES-free coating+ thermal treatment* (TCF)	DBES-containing coating (CHE)	DBES-containing coating + thermal treatment* (TCHE)
AELO [wt. (g)/wt.%]	100/78	100/78	100/67	100/67
DBES [wt. (g)/wt.%]	–	–	20/13	20/13
DHPA [wt. (g)/wt. %]	2.6/2	2.6/2	2.6/2	2.6/2
DMA [wt. (g)/wt.%]	26/20	26/20	26/18	26/18
Thickness	75 ± 5 μm	75 ± 5 μm	62 ± 8 μm	62 ± 8 μm

* 140 °C for 6 h.

each sample. It can be noticed that in the presence of DBES, the coatings thickness was slightly lower than that of the coatings without DBES. This can be explained by a lower viscosity of these formulations. Despite the difference in coating thickness, the impedance diagrams were not normalized by the thickness. The variation of the impedance modulus, induced by the difference in coating thickness would be comparatively negligible with respect to the high measured impedance values.

2.4. Characterization techniques

^{1}H NMR spectroscopy analyses were performed on a Bruker Avance 400 MHz spectrometer with a flip angle of 30°, an acquisition time of 4 s, a pulse delay of 1 s and a scan number of 4. Chemical shifts were reported in part per millions (ppm) relative to tetramethylsilane.

Thermogravimetric (TGA) measurements were achieved using a TGA Q50 apparatus from TA Instruments. Heating ramps were performed under air from 25 °C with a heating rate of 5 °C/min.

Differential scanning calorimetry (DSC) measurements were carried out with a DSC 204 Netzsch apparatus under inert atmosphere (N_2). The coating sample (approximately 7 mg) was deposited on a pierced aluminium crucible. Two heating ramps from 100 °C to 100 °C were successively performed with a heating rate of 10 °C/min. The cooling ramps were run at the same rate but were not considered in the present work. The glass transition temperature (T_g) was measured at the maximum of the derivative of the thermograms (second heating ramp). The uncertainty on the T_g determination, including repeatability on

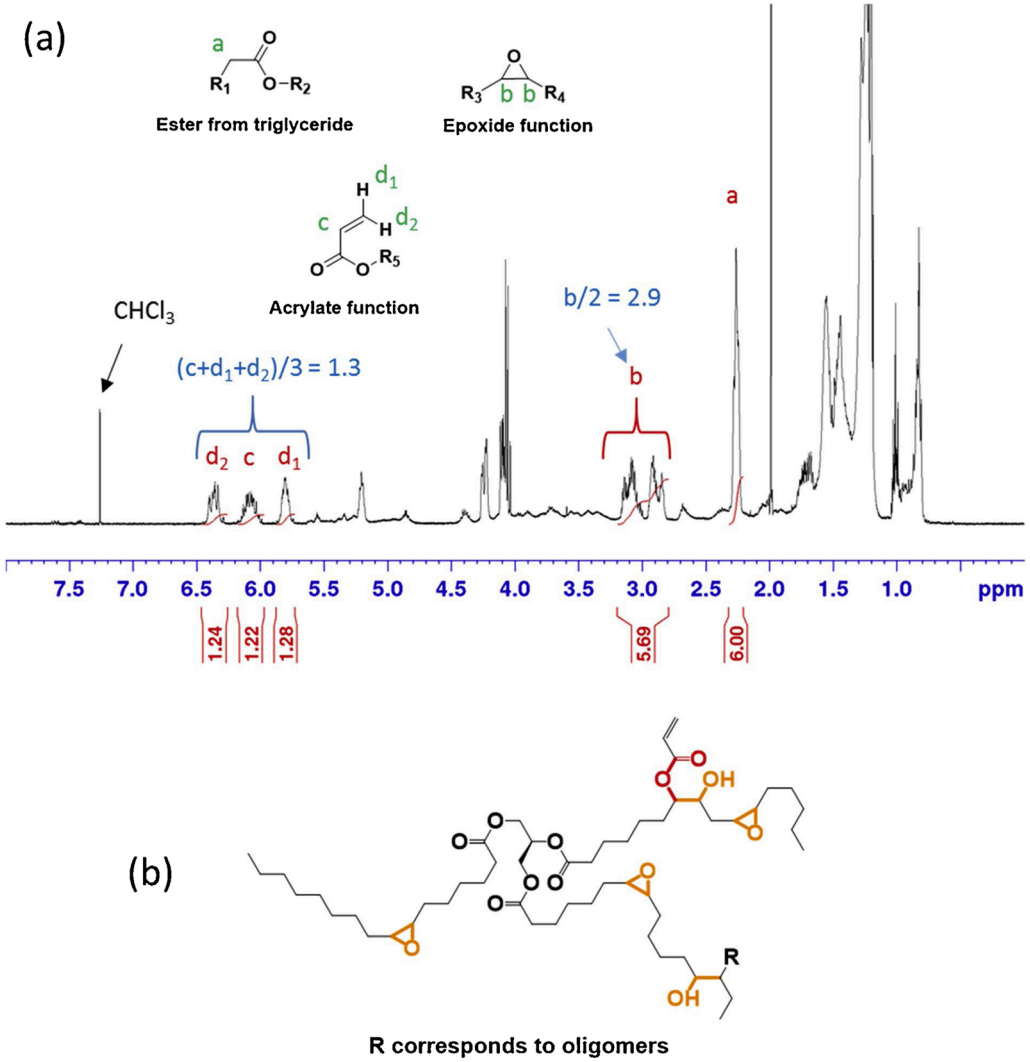


Fig. 2. (a) ^{1}H NMR spectrum of the synthesized AELO, and (b) AELO structure.

three samples, was evaluated at ±2 °C.

Electrochemical impedance measurements were performed with a conventional three-electrode cell, in which the AA3003 coated sample served as working electrode. A saturated calomel electrode and a graphite rod were used as reference and counter-electrode, respectively. All tests were carried out in a 0.5 M NaCl solution at room temperature. The coating area in contact with the electrolyte was 14.6 cm^2. Impedance measurements were performed with a Biologic VSP apparatus. The diagrams were obtained, under potentiostatic regulation, at the open circuit potential, using a 75 mV peak-to-peak sinusoidal voltage perturbation. For short immersion times, the diagrams were obtained in a reduced frequency range (100 kHz to 10 Hz) every 4 min during 90 min and then, for exposure times ranging from 2 h to 354 h, over a larger frequency range (100 kHz to 10 mHz). Reproducibility was checked using at least two different samples. A good reproducibility was observed and representative results are presented.

The impedance data analysis was performed using the EC-lab software provided with the EIS apparatus.

3. Results and discussion

3.1. AELO characterization

The AELO, synthesized via partial acrylation of the epoxidized linseed oil, was characterized by ^{1}H NMR in $CDCl_3$ to determine the amounts of acrylates and of remaining epoxides per triglyceride. The ^{1}H NMR spectrum of AELO is shown in Fig. 2a. The signal at 2.33 ppm (peak a) corresponds to the three CH_2 in alpha position of the ester functions and was used as reference to determine the amounts of grafted acrylates (peaks c, d_1 and d_2) and of unreacted epoxides per triglyceride (peak b). The average number of grafted acrylate functions per triglyceride was of 1.3. In radical polymerization process, one acrylate function reacts with two other monomers. Thus, a functionality of 1.3 was sufficient to produce a cross-linked system after curing. The average number of unreacted epoxides per triglyceride was determined to be 2.9, which was also sufficient to ensure an additional reaction. The AELO structure derived from the ^{1}H NMR analysis is given in Fig. 2b.

3.2. Thermal treatment: temperature selection

DBES dissociates when thermally treated to form sebacic acid and butyl vinyl ether (scheme (a) in Fig. 3). Then, the sebacic acid released into the coating can react with the epoxy groups of the AELO [38] as shown in Fig. 3 (scheme (b)). Thermogravimetric measurements were performed to determine the temperature at which DBES dissociates.

The thermogram in Fig. 4a shows a first mass loss (50 %), starting at about 150 °C, attributed to the DBES dissociation and evaporation of vinyl ether (P_{sat} of butyl vinyl ether 51 hPa at 20 °C). The second mass loss (50 %), between 200 °C and 260 °C, might be caused by evaporation and/or degradation of the released sebacic acid [35]. To select the temperature at which the DBES will be dissociated without significant evaporation/degradation of the released acid, isothermal TGA analyses were carried out at 125, 140 and 150 °C. Fig. 4b illustrates, as an example, the result obtained at 140 °C. During the first 100 min, a mass loss of about 50 % is observed, attributed to the DBES dissociation and vinyl ether evaporation. Then, a slow and linear mass loss is observed, attributed to the sebacic acid evaporation/degradation. From these two domains, both the dissociation time and the proportion of acid loss (in percent of the initial acid weight) during dissociation were determined. The corresponding values for the three temperatures are compared in Fig. 4c. It can be seen that for all temperatures, the amount of released acid which evaporates/degrades is not critical (≤16 %). The thermal treatment at 125 °C induces the lowest acid loss (9 %), but the longest dissociation time (370 min). In contrast, at 150 °C, the dissociation time is the shortest (70 min), but the acid loss is the highest (16 %). The treatment at 140 °C leads to a dissociation time (95 min) close to that obtained at 150 °C and to an acid loss (10 %) close to that obtained at 125 °C. Consequently, the temperature of 140 °C was chosen as a good compromise for the DBES dissociation and will then be used for the thermal treatment of the coating.

3.3. DSC characterisation

The free-standing films were characterized by DSC. Fig. 5 compares the thermograms of the homopolymerized AELO (Fig. 5a) to that of the CF coating (Fig. 5b). The corresponding derivatives are shown in Fig. 5c and d, respectively. The homopolymerized AELO was characterized by one T_g only, around 39 °C. In contrast, the CF coating displayed two T_gs: T_{g1} at 40 °C and T_{g2} at -20 °C, respectively. Two transitions have also been observed by Liu et al. [49] for an acrylated epoxidized soybean oil copolymer. The higher transition temperature was ascribed to the main copolymer chain, while the lower transition temperature was not discussed. The glass transition at about 40 °C (Fig. 5d) was identical to the one observed for the homopolymerized AELO. The copolymerization reactivity ratios of butyl acrylate (chosen as a model of AELO) and the reactive diluent (DMA) ($r_{Butyl\ acrylate}$ 1.01 and r_{DMA} 1.16) indicated a statistical copolymerization [50], making thus possible the use of the Fox equation to calculate the theoretical T_g of the copolymer. The amount of DHPA (2 wt.%) was considered negligible. The calculated T_g value (statistical copolymer composed of 79 wt.% of AELO (T_g 40

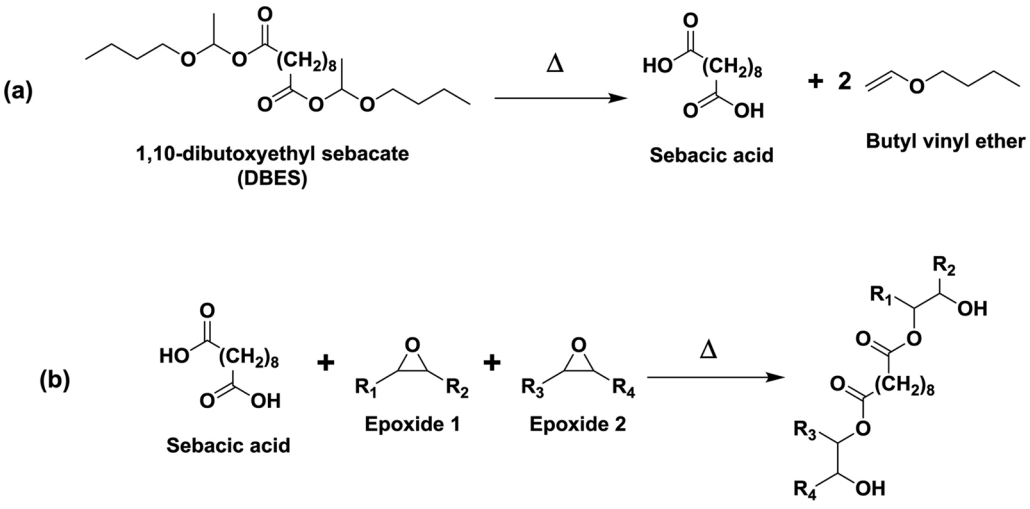


Fig. 3. Scheme of: (a) thermal dissociation of DBES and (b) epoxy-acid reaction.

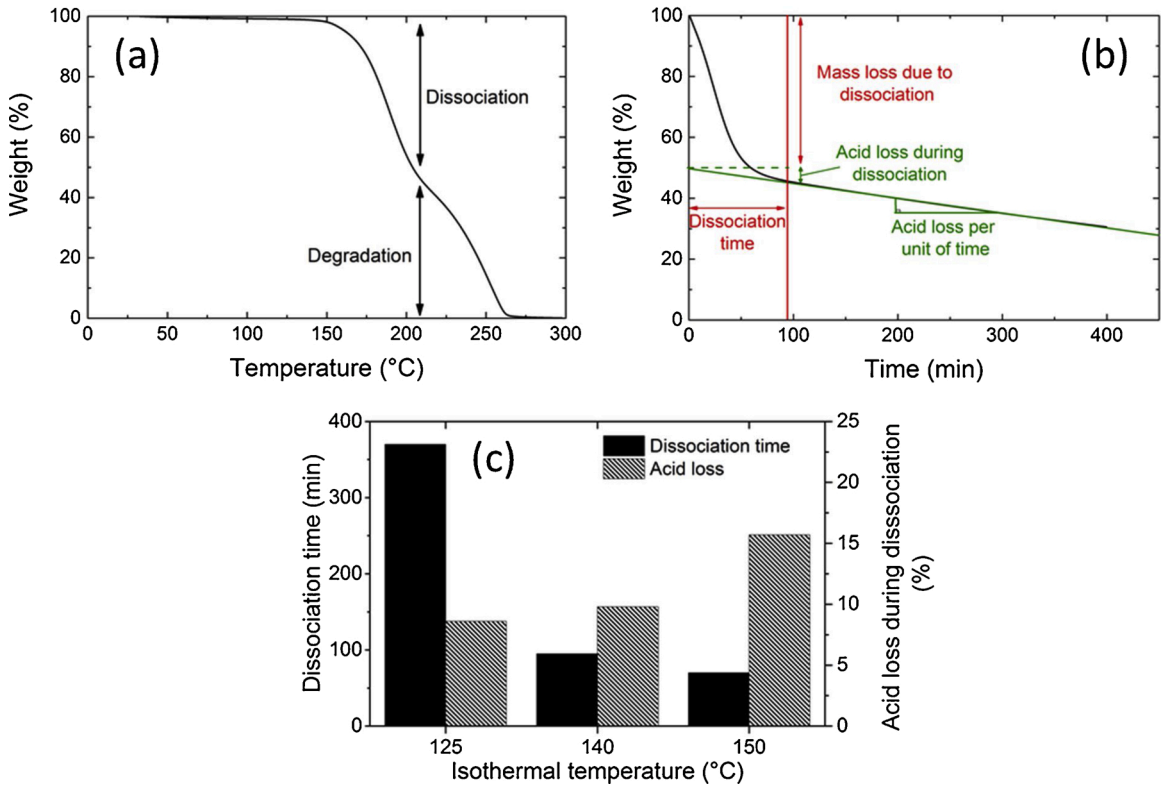


Fig. 4. (a) TGA thermogram (+5 °C/min) of the DBES, (b) TGA analysis of the DBES at 140 °C, and (c) dissociation time and acid loss of the DBES determined by TGA at 125, 140 and 150 °C.

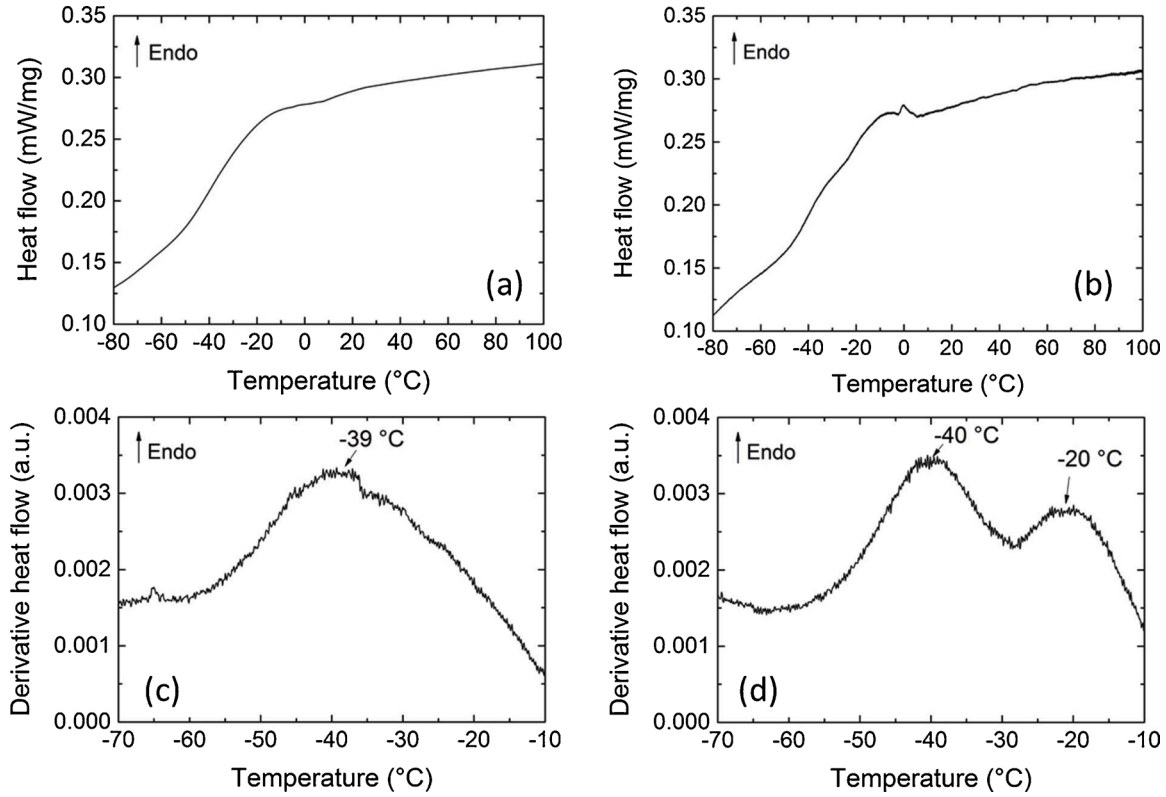


Fig. 5. DSC thermograms (+10 °C/min) of: (a) the homopolymerised AELO and (b) the CF coating; and derivatives of the thermograms: (c) of the homopolymerised AELO and (d) of the CF coating.

°C) and 21 wt.% of DMA (T_g of the homopolymer 118 °C [51])) was 18 °C. This agrees with the T_{g2} value (Fig. 5d).

The T_g values obtained from the DSC thermograms for the different coatings are reported in Table 2. The four coatings are characterized by two T_{gs}. For CF and TCF coatings, similar T_{g1} and T_{g2} values are observed. This indicates that, in the absence of the DBES, the thermal treatment did not modify the coating structure. The significantly lower T_g values for the CHE sample show the plasticizing effect of free DBES. For the thermally treated sample (TCHE coating), both T_{g1} and T_{g2} increased compared to the CHE sample (Table 2). This result might be explained by an antiplasticization effect due to both the loss of DBES and to an additional cross-linking (sebacic acid release and reaction with the AELO matrix (Fig. 3)). The T_g values of the TCHE coating are higher than those measured for the CF and the TCF coatings corroborating the additional cross-linking induced by the DBES dissociation.

3.4. Barrier properties and corrosion protection

The different coatings were characterized by EIS during immersion in a 0.5 M NaCl solution. The influence of the immersion time in the electrolytic solution, the addition of DBES, the thermal treatment, the appearance of corrosion and finally the healing effect of DBES will be successively presented and discussed.

3.4.1. Influence of the immersion time

Typical EIS diagrams are shown in Fig. 6 for the CF coating and for three immersion times. A single time constant can be observed on the impedance diagrams, which is classically associated to the response of an intact coating. The diagrams are almost superimposed for the three immersion times and the values of the impedance modulus at low frequency (on the plateau) are about 2 10^8 Ω cm^2. These results indicate efficient and stable barrier properties.

3.4.2. Influence of DBES addition and of the thermal treatment

The influence of the presence of DBES in the matrix (with and without thermal treatment) was also investigated by EIS measurements. Fig. 7 compares the impedance diagrams obtained for the four coatings after 24 h of immersion in a 0.5 M NaCl solution. Whatever the coatings, the diagrams are characterized by a single time constant characteristic of an intact coating. As noted above for the DSC results (same T_g values), there is no significant difference between the diagrams obtained for the CF and TCF samples (the diagrams are superimposed), which confirms that, in the absence of DBES, the thermal treatment did not modify the physical structure and the barrier properties of the coating. The impedance diagram of the CHE sample is quite similar to those obtained for CF and TCF coatings. Although the DSC results showed that the addition of DBES had a plasticizing effect (higher mobility of the polymer network), there is no repercussion on the barrier properties of the coating (CHE sample). This can be explained by the fact that the EIS experiments were performed at room temperature, far above the T_g of the samples (rubbery state), and for which the plasticization effect would become negligible. In Fig. 7, a noticeable increase of the impedance modulus at low frequency is observed for the TCHE sample (8 10^8 Ω cm^2) compared to the CHE sample (2 10^8 Ω cm^2). It would be linked to the additional cross-linking due to the DBES dissociation and to the reaction of the released sebacic acid with the matrix, as already mentioned. The impedance modulus at 50 mHz (on the plateau) was extracted from the impedance diagrams obtained for various immersion times in the 0.5 M NaCl solution. The values are reported in Fig. 8. The difference between the TCHE sample and the three other samples remains constant over immersion time in the 0.5 M NaCl solution showing that the greater barrier properties of TCHE sample are maintained over immersion time.

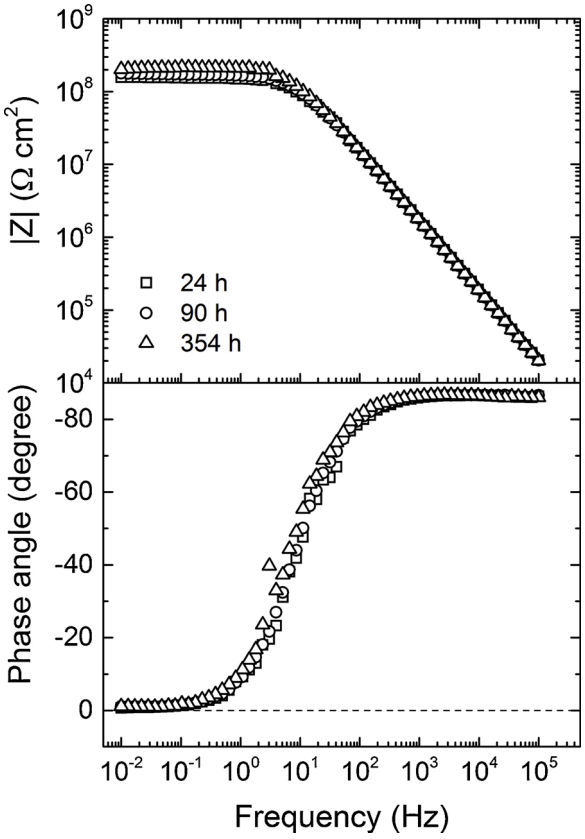


Fig. 6. Impedance diagrams (Bode plots) for the CF coating after 24 h, 90 h and 354 h of immersion in a 0.5 M NaCl solution.

3.4.3. Water uptake and diffusion coefficient

The water uptake for the different coatings was calculated from the high frequency part of the impedance diagrams. Coating capacitance (C_c) values were calculated at 10 kHz using Eq. (1) where Z'' correspond to the imaginary part of the impedance, f to the frequency and $|Z|$ to the impedance modulus.

$$C_c \quad \frac{Z''}{2\pi f |Z|^2} \tag{1}$$

Once the coating capacitance was known, the dielectric constant of the coating (ε_c) was calculated from the usual relationship:

$$\varepsilon_c \quad \frac{C_c \delta}{\varepsilon_0} \tag{2}$$

where ε_0 and δ represent, respectively, the vacuum permittivity and the thickness of the coating. First, the dielectric constant of the coating was plotted as a function of the square root of the immersion time, assuming a Fickian water uptake [52]. The dielectric constant of the coating at its

Table 2
Glass transition temperatures of the different coatings measured during the second heating ramp at 10 °C/min.

	DBES-free coating (CF)	DBES-free coating+ thermal treatment* (TCF)	DBES-containing coating (CHE)	DBES-containing coating + thermal treatment* (TCHE)
T_{g1} (°C)	−40	−38	−61	−26
T_{g2} (°C)	−20	−19	−35	−14

* 140 °C for 6 h.

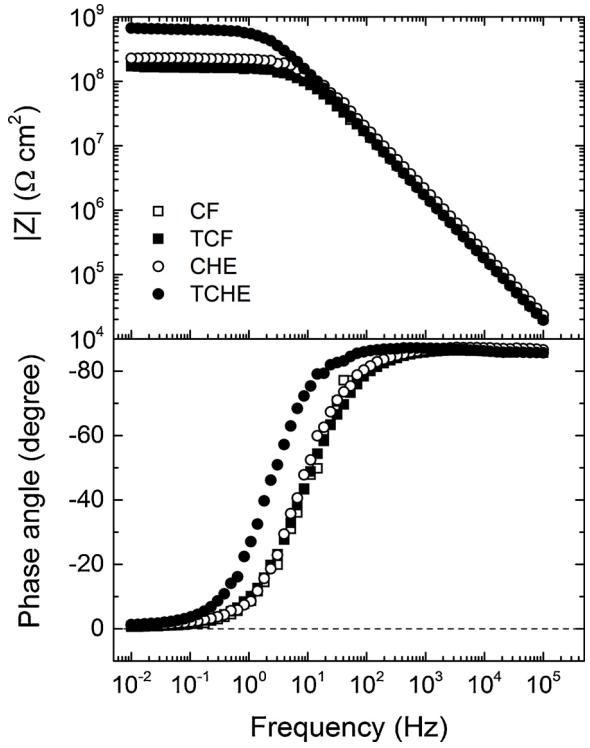


Fig. 7. Impedance diagrams (Bode plots) obtained for the four coatings after 24 h of immersion in a 0.5 M NaCl solution.

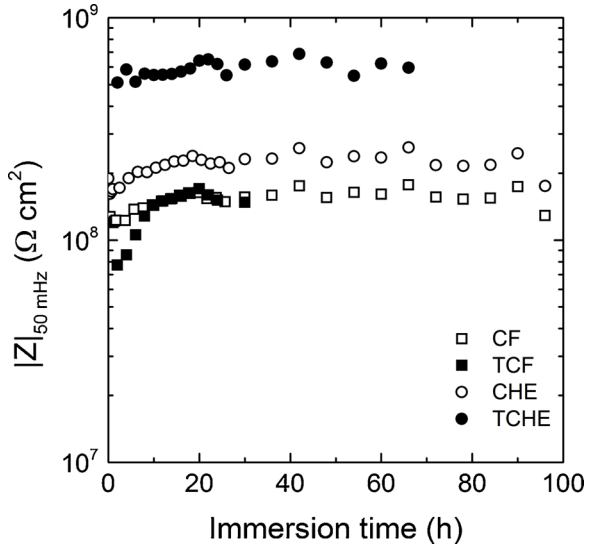


Fig. 8. Impedance modulus at low frequency (50 mHz) as a function of the immersion time in the 0.5 M NaCl solution for the four coatings.

initial state (dry coating) was determined at $t_{immersion}$ 0, from a linear extrapolation of the first points. Then, the volumic water uptake was calculated by using a linear rule of mixtures (Eq. (3)), taking into account the coating and the absorbed water [53–55].

$$\varnothing_{water} \quad \frac{\varepsilon_t \quad \varepsilon_{t0}}{\varepsilon_{water} \quad \varepsilon_{t0}} \tag{3}$$

Where ε_t is the permittivity of the coating at a given immersion time, ε_{t0} is the permittivity of the dry coating. The water permittivity, ε_{water} was assumed to be constant and the value used was 80 [56]. The comparison of the water uptake for the different coatings is shown in Fig. 9. The

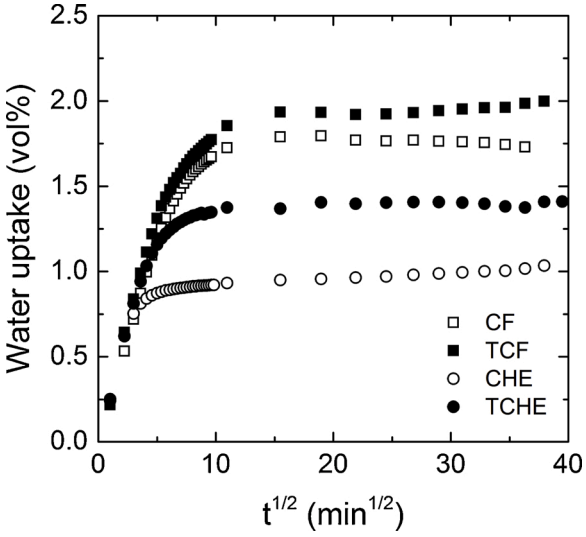


Fig. 9. Water uptake calculated from the impedance data using Eq. (3).

water uptake was calculated by using the mean coating thickness. The accuracy due to thickness variation is in the order of magnitude of the repeatability between two independent samples (about 0.1 vol.%).

For all the samples, the water uptake reaches a plateau, after about 2 h of immersion. On the plateau, the values of the water uptake vary between 1 and 2 % depending on the coating. These low water uptake values (considering the fact that the coatings were in the rubbery state [57]) can be explained by the overall hydrophobicity of the coating (oil-based polymer) which tends to repel water molecules. The CF and TCF formulations present similar water uptake values of about 2 vol.%, in agreement with the fact that, in the absence of DBES, the thermal treatment has no effect on the matrix. These two samples absorbed more water compared to the CHE sample (around 1 vol.%). This result might be explained by the fact that DBES is a water-immiscible compound, thus increasing the overall hydrophobicity of the CHE coating and preventing water ingress. The water uptake for the TCHE sample (around 1.2 vol.%) is higher (+0.4 vol.%) than that determined for the CHE coating. This increase could be attributed to the presence of hydrophilic functions (hydroxyl groups) [38] in the AELO matrix after the epoxy-acid reaction as it can be seen in the scheme in Fig. 3b. The water diffusion coefficient, *D*, was estimated from Fig. 9 using Eq. (4) [58].

$$D \quad \frac{0.049}{\left(\frac{t}{\delta^2}\right)^{1/2}} \tag{4}$$

The *D* values are in the same order of magnitude for all the coatings (4 10^{-13} m^2 s^{-1}). Similar diffusion coefficients have been reported for acrylate based-matrix using gravimetric measurements [59–61].

3.4.4. *Appearance of corrosion*

At longer immersion time, a change in the impedance diagrams was observed for several formulations. The diagrams were characterized by the presence of a new time constant which can be linked to the occurrence of corrosion. However, the appearance of this phenomenon presented a random character, even for the same sample (for example, Figs. 6 and 10 can be compared for the CF sample). This random event might be attributed to weak zones in the coatings (due to the samples preparation) facilitating the penetration of aggressive species, particularly Cl^-, triggering the corrosion of the AA3003. An example of the EIS diagrams for the CF coating obtained with the occurrence of corrosion is shown in Fig. 10. For this sample, the corrosion appeared between 24 h and 87 h. A slow evolution of the diagrams is observed between 87 h and 183 h of immersion. The impedance diagrams were fitted by the two

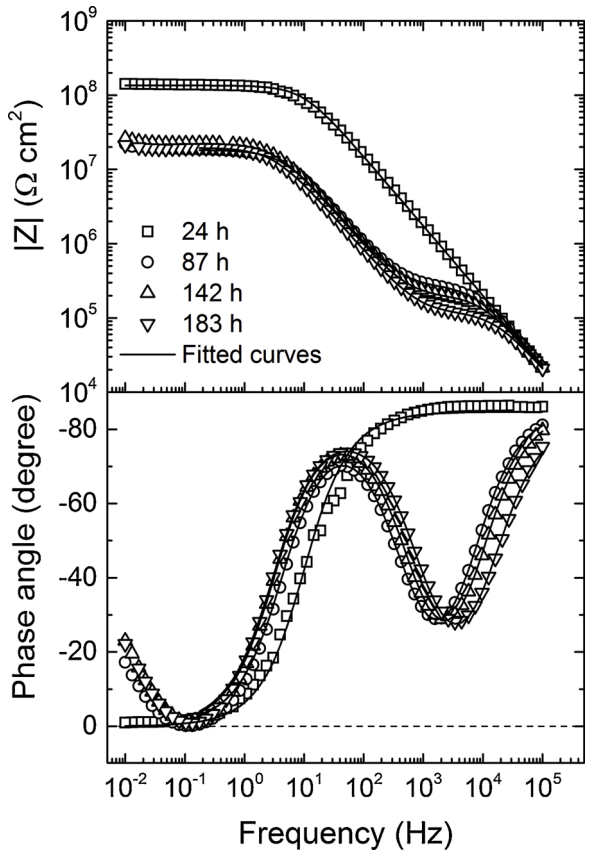


Fig. 10. Impedance diagrams (Bode plots) obtained for the CF coating after different immersion times in a 0.5 M NaCl solution (corrosion appeared between 24 h and 87 h of immersion).

equivalent electrical circuits, commonly used to analyse intact and damaged coatings (Fig. 11) [43,44]. The diagram obtained for 24 h of immersion was fitted with a non-ideal RC circuit whereas the curves obtained for 87 h, 142 h and 183 h were fitted using two non-ideal RC circuits to analyse the two time constants. The values of the parameters, extracted from the diagrams, are reported in Table 3.

When corrosion occurred, a third time constant is observed in the low frequency range (100-10 mHz). This time constant is linked to the corrosion processes occurring at the AA3003/coating interface. In neutral solution, the cathodic reaction (oxygen reduction) is controlled by diffusion. This process is generally characterized by a time constant in the low frequency range [62]. Here, only the beginning of this third time constant can be seen. For sake of simplicity, the impedance diagrams were analysed until 1 Hz or 100 mHz, only.

In the equivalent circuits, R_e, is the electrolyte resistance, R_{pore} is the electrolyte resistance in the pores and R_t corresponds to the charge transfer resistance, linked to the corrosion process. A constant phase element (*CPE*) was used instead of a capacitance to take into account the non-ideal behaviour of the interface. The *CPE* is given by:

$$Z_{CPE} \quad \frac{1}{Q\,(j\omega)^{\alpha}} \tag{5}$$

Where α is related to the angle of rotation of a purely capacitive line on the complex plane plots and Q is a constant expressed in Ω^{-1} cm^{-2} s$^{\alpha}$. Q_c and α_c correspond to the CPE of the coating and Q_{dl} and α_{dl} to the CPE of the double layer capacitance.

R_{pore} and R_t (Table 3) kept relatively high values after the appearance of corrosion. This suggests that the corrosion process was limited to a small area. This is also in agreement with the low Q_{dl} values. A double layer capacitance on bare metal substrate is usually around 50–100 10^{-6} F cm^{-2}. Even if Q_{dl} values do not strictly correspond to capacitance values (α_{dl} 0.92 instead of 1 for a pure capacitance), the huge difference between 50–100 10^{-6} F cm^{-2} and the Q_{dl} values (Table 3) confirmed the small-corroded area. At the end of the test, after the removal of the electrolyte, a single localized spot was visible on the surface. The Q_{dl} values, which depend on the exposed metal surface area, increased slowly between 87 h and 183 h, indicating a slow evolution of the corrosion process, which in turn indicates that the appearance of corrosion did not lead to coating delamination and/or corrosion propagation. The fact that the appearance of corrosion did not induce a rapid degradation of the AA3003/coating interface, suggests a significant adhesion of the coating on the metal substrate [23]. This can be attributed to the use of DHPA, as adhesion promoter. It is important to emphasize that without DHPA and DMA, all coatings easily peeled off from the AA3003 substrate.

Fig. 12 shows some impedance diagrams obtained for the CHE and TCHE coatings. Corrosion appeared between 90 h and 162 h for the CHE sample and between 66 h and 72 h for the TCHE sample. These impedance results underline the random appearance of corrosion. It is noteworthy that, for both systems, after the corrosion initiation, there is only a slight evolution of the impedance diagrams with increasing immersion time in the aggressive solution (Fig. 12). Again, this suggests the beneficial and important role of the adhesion promoter, independently of the presence of DBES and of the thermal treatment.

To investigate a potential healing effect of DBES, impedance diagrams of the CHE coating were obtained before and after the thermal treatment (same sample). The impedance diagrams are shown in Fig. 13a and b before and after the thermal treatment, respectively. For this sample, the corrosion appeared relatively early after immersion: the

Table 3
Parameters values obtained from the impedance diagrams for the CF coating (Fig. 10) by using the equivalent electrical circuits given in Fig. 11.

Immersion time	24 h	87 h	142 h	183 h
R_{pore} (Ω cm^2)	1.2 10^8	2.9 10^5	2.1 10^5	1.3 10^5
Q_c (F s$^{(\alpha\ 1)}$ cm^{-2})	1.5 10^{-10}	1.4 10^{-10}	1.5 10^{-10}	2.0 10^{-10}
α_c	0.95	0.95	0.95	0.95
R_t (Ω cm^2)	/	1.8 10^7	2.2 10^7	1.9 10^7
Q_{dl} (F s$^{(\alpha\ 1)}$ cm^{-2})	/	2.4 10^{-9}	2.6 10^{-9}	3.2 10^{-9}
α_{dl}	/	0.92	0.92	0.92

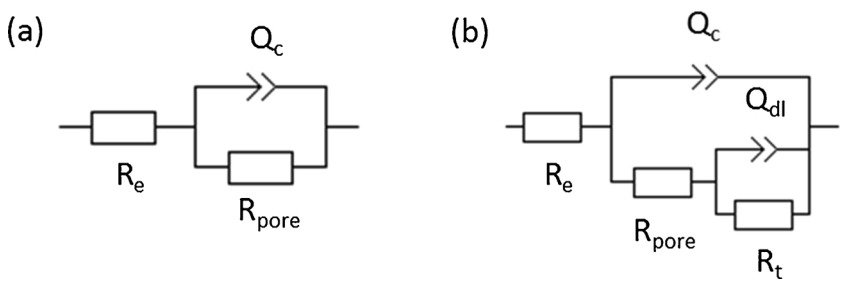


Fig. 11. Equivalent electrical circuits corresponding to: a) an intact coating and b) a damaged coating and used to analyse the impedance data in Figs. 10 and 13.

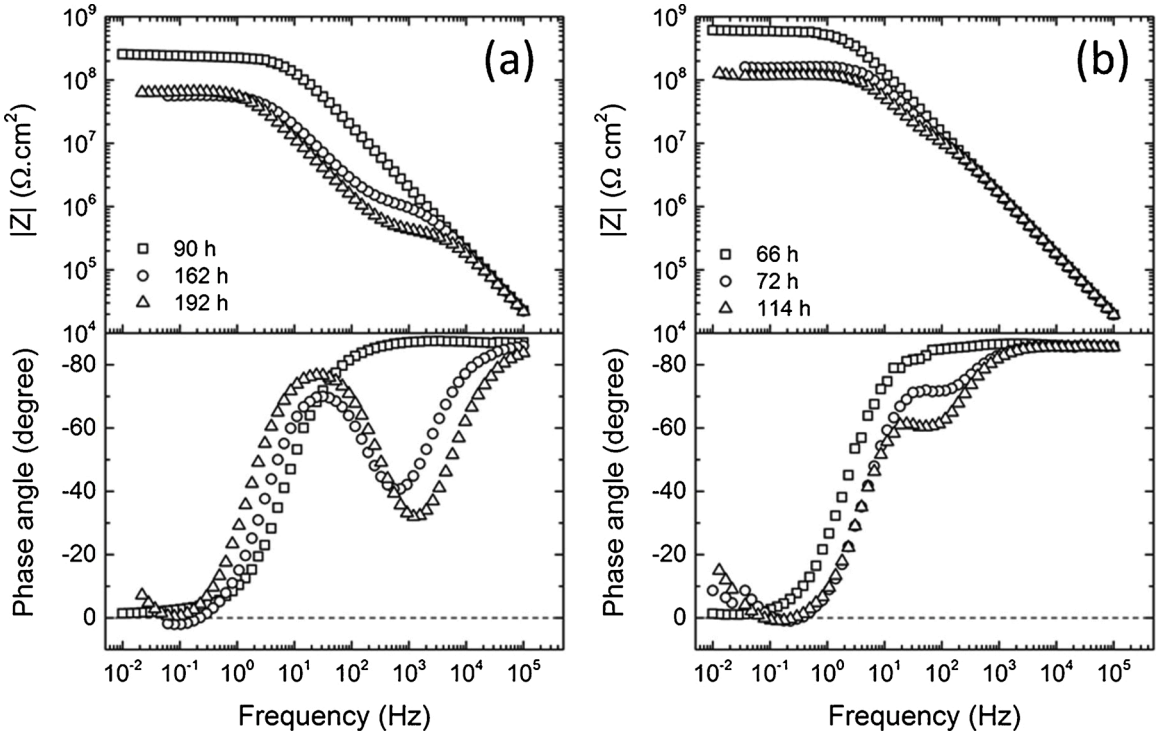


Fig. 12. Impedance diagrams (Bode plots) obtained for (a) the CHE and (b) the TCHE coatings after different immersion times in a 0.5 M NaCl solution.

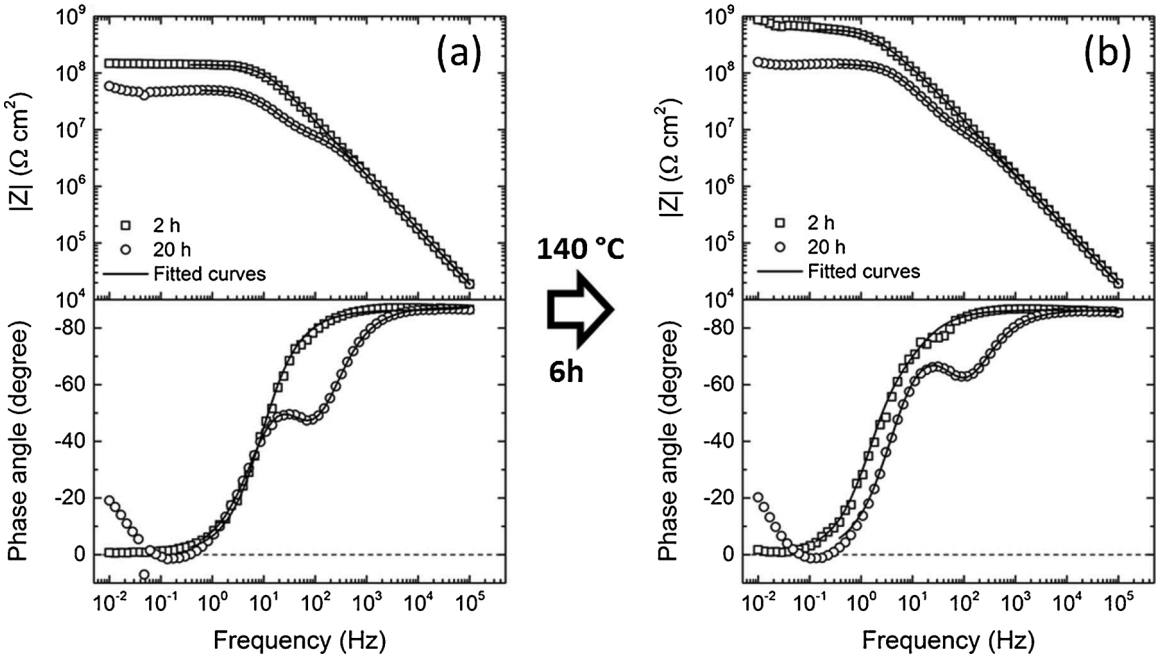


Fig. 13. Impedance diagrams (Bode plots) obtained for the CHE coating during immersion in a 0.5 M NaCl solution (a) before the thermal treatment and (b) after the thermal treatment on the same sample.

diagram presents two time constants after 20 h of immersion, only. The experiment was stopped after 20 h of immersion and the thermal treatment was applied to the CHE sample. Then, this thermally-treated coating was again immersed in the NaCl solution and impedance diagrams were obtained after 2 h and 20 h of immersion in the 0.5 M NaCl solution (Fig. 13b). The diagrams were fitted by the equivalent electrical circuits presented in Fig. 11. The extracted parameters are compared in Table 4. The R_{pore} value of the CHE sample before the thermal treatment and in the absence of corrosion was of 1.4 10^8 Ω cm^2. This value decreased with the appearance of corrosion (0.1 10^8 Ω cm^2) but, after the thermal treatment and 2 h of immersion in the NaCl solution, the R_{pore} value is higher (3.6 10^8 Ω cm^2) than that measured after 2 h of immersion before the thermal treatment. In addition, even if the two time constants are observed after the thermal treatment (Fig. 13b), the Q_{dl} value was about three times lower than that obtained for 20 h of immersion, before the thermal treatment. These observations, on the same sample, support a repairing effect of the polymer matrix. Due to the presence of DBES, the thermal treatment induced an additional

Table 4
Parameters values obtained from the impedance diagrams for the same CHE sample before and after the thermal treatment (Fig. 13) by using the equivalent electrical circuits given in Fig. 11.

CHE sample	Before the thermal treatment 2 h	Before the thermal treatment 20 h	After the thermal treatment 2 h	After the thermal treatment 20 h
R_{pore} (Ω cm^2)	1.4 10^8	0.10 10^8	3.6 10^8	0.14 10^8
Q_c (F $s^{(\alpha\ 1)}$ cm^{-2})	1.4 10^{-10}	1.2 10^{-10}	1.4 10^{-10}	1.4 10^{-10}
α_c	0.96	0.97	0.96	0.96
R_t (Ω cm^2)	/	0.4 10^8	2.3 10^8	1.3 10^8
Q_{dl} (F $s^{(\alpha\ 1)}$ cm^{-2})	/	6.2 10^{-10}	1.9 10^{-10}	2.1 10^{-10}
α_{dl}	/	0.93	0.97	0.97

cross-linking and the self-healing of small defects or heterogeneities in the coating.

To summarize, it was shown that, in the absence of DBES, the thermal treatment did not modify the coating properties. In contrast, when DBES was introduced into the coating, the thermal treatment led to: (i) an increase of the glass transition temperatures (T_{g1} and T_{g2}), (ii) an increase of the impedance modulus (higher barrier properties) and (iii) a slight increase of the water uptake during immersion in the NaCl solution. All these modifications were attributed to the reaction of the released acid from the DBES hemiacetal ester functions with the epoxide functions worn by the acrylated epoxidized linseed oil. EIS results showed that this additional cross-linking can heal the bio-based matrix (small defects or heterogeneities in the coating), which partially restored its protective efficiency.

4. Conclusions

The corrosion protection of an AA3003 substrate by a partially bio-based coating prepared from copolymerization of a partially acrylated epoxidized linseed oil with *N*,*N*-dimethyl acrylamide and (3,4-dihydroxyphenethyl)acrylamide was studied by EIS. In the absence of DBES, this coating showed interesting barrier properties, high stability and low water uptake (due to its high hydrophobicity) during immersion in the NaCl solution. The incorporation of DBES did not lead to significant modifications of the barrier properties of the coating, but lowered the T_g (plasticization) and the water uptake (higher hydrophobicity). The ability of DBES to induce additional cross-linking with latent epoxide functions under thermal treatment was demonstrated both by EIS measurements (higher barrier effect) and DSC analysis (higher T_g values). After the appearance of corrosion, the thermal treatment of the partially bio-based coating allowed a partial healing of the matrix and the barrier properties were at least partially restored, thereby demonstrating that the DBES was responsible for the observed effect (self-healing). After the corrosion initiation, there was no delamination of the coatings, which was indicative of a significant adhesion of the coatings on the AA3003 substrate. This can be attributed to the improved affinity of the formulation to the substrate brought by (3,4-dihydroxyphenethyl) acrylamide.

The good performance of these coatings from vegetable oils without fillers or corrosion inhibitors shows the feasibility of developing new bio-based protective coatings. The promising effect of hemiacetal ester functions could be used in the development of self-healing systems.

Author contributions

David Boucher Conceptualization, Data curation; Formal analysis, Investigation, Writing - original draft.

Nicolas Caussé Conceptualization, Formal analysis, Methodology, Project administration, Supervision, Validation, Writing - review & editing.

Nadine Pébère Conceptualization, Formal analysis, Methodology, Project administration, Supervision, Validation, Writing - review & editing.

Vincent Ladmiral Conceptualization, Project administration, Supervision, Validation, Writing - review & editing.

Claire Negrell Conceptualization, Project administration, Supervision, Validation, Writing - review & editing.

Declaration of Competing Interest

The authors declare that they have no known competing financial interests or personal relationships that could have appeared to influence the work reported in this paper.

Acknowledgements

This project was supported by Chimie Balard Cirimat Carnot Institute through the ANR program N°16 CARN 0008-01. The authors gratefully acknowledge Hobum Oleochemical GmbH for kindly providing the epoxidized linseed oil (Merginate ELO).

References

[1] S. Doley, S.K. Dolui, Solvent and catalyst-free synthesis of sunflower oil based polyurethane through non-isocyanate route and its coatings properties, Eur. Polym. J. 102 (2018) 161–168, https://doi.org/10.1016/j.eurpolymj.2018.03.030.
[2] T. Ghosh, N. Karak, Mechanically robust hydrophobic interpenetrating polymer network-based nanocomposite of hyperbranched polyurethane and polystyrene as an effective anticorrosive coating, New J. Chem. 44 (2020) 5980–5994, https://doi.org/10.1039/D0NJ00322K.
[3] M.M. Ariffin, M.M. Aung, L.C. Abdullah, M.Z. Salleh, Assessment of corrosion protection and performance of bio-based polyurethane acrylate incorporated with nano zinc oxide coating, Polym. Test. 87 (2020), 106526, https://doi.org/10.1016/j.polymertesting.2020.106526.
[4] J.V. Nardeli, C.S. Fugivara, M. Taryba, M.F. Montemor, S.J.L. Ribeiro, A. V. Benedetti, Novel healing coatings based on natural-derived polyurethane modified with tannins for corrosion protection of AA2024-T3, Corros. Sci. 162 (2020), 108213, https://doi.org/10.1016/j.corsci.2019.108213.
[5] J.V. Nardeli, C.S. Fugivara, M. Taryba, M.F. Montemor, A.V. Benedetti, Biobased self-healing polyurethane coating with Zn micro-flakes for corrosion protection of AA7475, Chem. Eng. J. 404 (2021), 126478, https://doi.org/10.1016/j.cej.2020.126478.
[6] Y. Zhang, X. Liu, G. Zhan, Q. Zhuang, R. Zhang, J. Qian, Study on the synergistic anticorrosion property of a fully bio-based polybenzoxazine copolymer resin, Eur. Polym. J. 119 (2019) 477–486, https://doi.org/10.1016/j.eurpolymj.2019.07.020.
[7] X. Liu, Z. Li, G. Zhan, Y. Wu, Q. Zhuang, Bio-based benzoxazines based on sesamol: synthesis and properties, J. Appl. Polym. Sci. 136 (2019), 48255, https://doi.org/10.1002/app.48255.
[8] A. Hariharan, P. Prabunathan, A. Kumaravel, M. Manoj, M. Alagar, Bio-based polybenzoxazine composites for oil-water separation, sound absorption and corrosion resistance applications, Polym. Test. 86 (2020), 106443, https://doi.org/10.1016/j.polymertesting.2020.106443.
[9] A. Hadzich, G.A. Gross, M. Leimbach, A. Ispas, A. Bund, S. Flores, Effect of polyalcohols on the anticorrosive behaviour of alkyd coatings prepared with drying oils, Prog. Org. Coat. 145 (2020), 105671, https://doi.org/10.1016/j.porgcoat.2020.105671.
[10] D.M. Patil, G.A. Phalak, S.T. Mhaske, Design and synthesis of bio-based epoxidized alkyd resin for anti-corrosive coating application, Iran. Polym. J. 27 (2018) 709–719, https://doi.org/10.1007/s13726-018-0646-1.
[11] I.M. Mousaa, H. Radi, Photosynthesis of anticorrosive protective coatings for steel substrate based on acrylated oil containing unsaturated amino acid compounds, Prog. Org. Coat. 107 (2017) 18–28, https://doi.org/10.1016/j.porgcoat.2017.03.006.
[12] H. Zhao, J. Ding, H. Yu, Advanced bio-based UV-curable anticorrosive coatings reinforced by hBN, ChemistrySelect 3 (2018) 11277–11283, https://doi.org/10.1002/slct.201802079.
[13] M.M. Aung, W.J. Li, H.N. Lim, Improvement of anticorrosion coating properties in bio-based polymer epoxy acrylate incorporated with nano zinc oxide particles, Ind. Eng. Chem. Res. 59 (2020) 1753–1763, https://doi.org/10.1021/acs.iecr.9b05639.
[14] I.M. Mousaa, Synthesis and performance of bio-based unsaturated oligomer and containing gum arabic as a novel protective steel coating under UV irradiation,

Prog. Org. Coat. 139 (2020), 105400, https://doi.org/10.1016/j.porgcoat.2019.105400.
[15] L.R.R. da Silva, F. Avelino, O.B.F. Diogenes, V. de O.F. Sales, K.T. da Silva, W. S. Araujo, S.E. Mazzetto, D. Lomonaco, Development of BPA-free anticorrosive epoxy coatings from agroindustrial waste, Prog. Org. Coat. 139 (2020), 105449, https://doi.org/10.1016/j.porgcoat.2019.105449.
[16] C. Coquery, F. Carosio, C. Negrell, N. Caussé, N. Pébère, G. David, New bio-based phosphorylated chitosan/alginate protective coatings on aluminum alloy obtained by the LbL technique, Surf. Interfaces 16 (2019) 59–66, https://doi.org/10.1016/j.surfin.2019.04.010.
[17] C. Zhang, T.F. Garrison, S.A. Madbouly, M.R. Kessler, Recent advances in vegetable oil-based polymers and their composites, Prog. Polym. Sci. 71 (2017) 91–143, https://doi.org/10.1016/j.progpolymsci.2016.12.009.
[18] S.F. Thames, H. Yu, Cationic UV-cured coatings of epoxide-containing vegetable oils, Surf. Coat. Technol. 115 (1999) 208–214, https://doi.org/10.1016/S0257-8972(99)00244-3.
[19] S. Ahmad, F. Naqvi, E. Sharmin, K.L. Verma, Development of amine-acid cured Annona squamosa oil epoxy anticorrosive polymeric coatings, Prog. Org. Coat. 55 (2006) 268–275, https://doi.org/10.1016/j.porgcoat.2005.11.013.
[20] C. Noè, L. Iannucci, S. Malburet, A. Graillot, M. Sangermano, S. Grassini, New UV-curable anticorrosion coatings from vegetable oils, Macromol. Mater. Eng. (2021), 2100029, https://doi.org/10.1002/mame.202100029.
[21] O. Negele, W. Funke, Internal stress and wet adhesion of organic coatings, Prog. Org. Coat. 28 (1996) 285–289, https://doi.org/10.1016/0300-9440(95)00606-0.
[22] P. Taheri, H. Terryn, J.M.C. Mol, Studying interfacial bonding at buried polymer–zinc interfaces, Prog. Org. Coat. 89 (2015) 323–331, https://doi.org/10.1016/j.porgcoat.2015.03.017.
[23] F. Deflorian, L. Fedrizzi, Adhesion characterization of protective organic coatings by electrochemical impedance spectroscopy, J. Adhes. Sci. Technol. 13 (1999) 629–645, https://doi.org/10.1163/156856199X00154.
[24] S. Seo, D.W. Lee, J.S. Ahn, K. Cunha, E. Filippidi, S.W. Ju, E. Shin, B.-S. Kim, Z. A. Levine, R.D. Lins, J.N. Israelachvili, J.H. Waite, M.T. Valentine, J.E. Shea, B. K. Ahn, Significant performance enhancement of polymer resins by bioinspired dynamic bonding, Adv. Mater. 29 (2017), 1703026, https://doi.org/10.1002/adma.201703026.
[25] J. Saiz-Poseu, J. Mancebo-Aracil, F. Nador, F. Busqué, D. Ruiz-Molina, The chemistry behind catechol-based adhesion, Angew. Chemie Int. Ed. 58 (2019) 696–714, https://doi.org/10.1002/anie.201801063.
[26] N. Patil, C. Jérôme, C. Detrembleur, Recent advances in the synthesis of catechol-derived (bio)polymers for applications in energy storage and environment, Prog. Polym. Sci. 82 (2018) 34–91, https://doi.org/10.1016/j.progpolymsci.2018.04.002.
[27] N. Patil, C. Falentin-Daudré, C. Jérôme, C. Detrembleur, Mussel-inspired protein-repelling ambivalent block copolymers: controlled synthesis and characterization, Polym. Chem. 6 (2015) 2919–2933, https://doi.org/10.1039/C5PY00127G.
[28] P. Kord Forooshani, B.P. Lee, Recent approaches in designing bioadhesive materials inspired by mussel adhesive protein, J. Polym. Sci. Part A Polym. Chem. 55 (2017) 9–33, https://doi.org/10.1002/pola.28368.
[29] Y. Cui, S. Song, Y. Tang, Y. Chen, H. Yang, B. Yang, J. Huang, Decoupling the roles of the catechol content from those of glass transition temperature and dynamic mechanical modulus in determining self-healing and anti-corrosion of mussel-inspired polymers, Polymer (Guildf.) 185 (2019), 121928, https://doi.org/10.1016/j.polymer.2019.121928.
[30] K.A. Yasakau, J. Tedim, M.L. Zheludkevich, M.G.S. Ferreira, Smart self-healing coatings for corrosion protection of aluminium alloys. Handb. Smart Coatings Mater. Prot., Elsevier, 2014, pp. 224–274, https://doi.org/10.1533/9780857096883.2.224.
[31] F. Zhang, P. Ju, M. Pan, D. Zhang, Y. Huang, G. Li, X. Li, Self-healing mechanisms in smart protective coatings: a review, Corros. Sci. 144 (2018) 74–88, https://doi.org/10.1016/j.corsci.2018.08.005.
[32] D. Crespy, K. Landfester, J. Fickert, M. Rohwerder, Self-healing for anticorrosion based on encapsulated healing agents, Adv. Polym. Sci. (2016) 219–245, https://doi.org/10.1007/12_2015_342.
[33] K. Urdl, A. Kandelbauer, W. Kern, U. Müller, M. Thebault, E. Zikulnig-Rusch, Self-healing of densely crosslinked thermoset polymers - a critical review, Prog. Org. Coat. 104 (2017) 232–249, https://doi.org/10.1016/j.porgcoat.2016.11.010.
[34] G. Cui, Z. Bi, S. Wang, J. Liu, X. Xing, Z. Li, B. Wang, A comprehensive review on smart anti-corrosive coatings, Prog. Org. Coat. 148 (2020), 105821, https://doi.org/10.1016/j.porgcoat.2020.105821.
[35] H. Otsuka, T. Endo, Poly(hemiacetal ester)s: new class of polymers with thermally dissociative units in the main chain, Macromolecules 32 (1999) 9059–9061, https://doi.org/10.1021/ma9909408.
[36] H. Otsuka, H. Fujiwara, T. Endo, Thermal dissociation behavior of polymers with hemiacetal ester moieties in the side chain: the effect of structure on dissociation temperature, J. Polym. Sci. Part A Polym. Chem. 37 (1999) 4478–4482, https://doi.org/10.1002/(SICI)1099-0518(19991215)37:24<4478::AID-POLA2>3.0.CO;2-R.
[37] T. Yamamoto, M. Ishidoya, New thermosetting coatings using blocked carboxyl groups, Prog. Org. Coat. 40 (2000) 267–273, https://doi.org/10.1016/S0300-9440(99)00086-7.
[38] C.S. Kovash, E. Pavlacky, S. Selvakumar, M.P. Sibi, D.C. Webster, Thermoset coatings from epoxidized sucrose soyate and blocked, bio-based dicarboxylic acids, ChemSusChem 7 (2014) 2289–2294, https://doi.org/10.1002/cssc.201402091.
[39] H. Komatsu, T. Hino, T. Endo, Novel thermally latent self-crosslinkable copolymers bearing oxetane and hemiacetal ester moieties: the synthesis, self-crosslinking behavior, and thermal properties, J. Polym. Sci. Part A: Polym. Chem. 43 (2005) 4260–4270, https://doi.org/10.1002/pola.20910.
[40] H. Komatsu, B. Ochiai, T. Hino, T. Endo, Model reaction for thermally latent curing through addition of hemiacetal ester and epoxide by schiff-base–zinc halide complexes, J. Polym. Sci. Part A: Polym. Chem. 45 (2007) 3370–3379, https://doi.org/10.1002/pola.22087.
[41] H. Komatsu, B. Ochiai, T. Hino, T. Endo, Thermally latent reaction of hemiacetal ester with epoxide controlled by Schiff-base-zinc chloride complexes with tunable catalytic activity, J. Mol. Catal. A Chem. 273 (2007) 289–297, https://doi.org/10.1016/j.molcata.2007.04.016.
[42] H. Komatsu, B. Ochiai, T. Endo, Thermally latent synthesis of networked polymers from multifunctional hemiacetal ester and diepoxide catalyzed by Schiff-base-zinc chloride complex, J. Polym. Sci. Part A: Polym. Chem. 46 (2008) 3682–3689, https://doi.org/10.1002/pola.22709.
[43] I.C.P. Margarit-Mattos, EIS and organic coatings performance: revisiting some key points, Electrochim. Acta 354 (2020), 136725, https://doi.org/10.1016/j.electacta.2020.136725.
[44] A. Amirudin, D. Thierry, Application of electrochemical impedance spectroscopy to study the degradation of polymer-coated metals, Prog. Org. Coat. 26 (1995) 1–28, https://doi.org/10.1016/0300-9440(95)00581-1.
[45] J. La Scala, R.P. Wool, Fundamental thermo-mechanical property modeling of triglyceride-based thermosetting resins, J. Appl. Polym. Sci. 127 (2013) 1812–1826, https://doi.org/10.1002/app.37927.
[46] D. Boucher, J. Madsen, N. Caussé, N. Pébère, V. Ladmiral, C. Negrell, Hemiacetal ester exchanges, study of reaction conditions and mechanistic pathway, Reactions 1 (2020) 89–101, https://doi.org/10.3390/reactions1020008.
[47] L. Huang, Y. Li, J. Yang, Z. Zeng, Y. Chen, Self-initiated photopolymerization of hyperbranched acrylates, Polymer (Guildf.) 50 (2009) 4325–4333, https://doi.org/10.1016/j.polymer.2009.07.004.
[48] H. Wang, H.R. Brown, Self-initiated photopolymerization and photografting of acrylic monomers, Macromol. Rapid Commun. 25 (2004) 1095–1099, https://doi.org/10.1002/marc.200400010.
[49] K. Liu, S.A. Madbouly, M.R. Kessler, Biorenewable thermosetting copolymer based on soybean oil and eugenol, Eur. Polym. J. 69 (2015) 16–28, https://doi.org/10.1016/j.eurpolymj.2015.05.021.
[50] D. Neugebauer, K. Matyjaszewski, Copolymerization of N, N -dimethylacrylamide with n -butyl acrylate via atom transfer radical polymerization, Macromolecules 36 (2003) 2598–2603, https://doi.org/10.1021/ma025883o.
[51] K. Bauri, S.G. Roy, S. Arora, R.K. Dey, A. Goswami, G. Madras, P. De, Thermal degradation kinetics of thermoresponsive poly(*N*-isopropylacrylamide-*co*-*N*,*N*-dimethylacrylamide) copolymers prepared via RAFT polymerization, J. Therm. Anal. Calorim. 111 (2013) 753–761, https://doi.org/10.1007/s10973-012-2344-0.
[52] E.P.M. van Westing, G.M. Ferrari, J.H.W. de Wit, The determination of coating performance with impedance measurements-II. Water uptake of coatings, Corros. Sci. 36 (1994) 957–977, https://doi.org/10.1016/0010-938X(94)90197-X.
[53] A.S. Castela, A.M. Simoes, An impedance model for the estimation of water absorption in organic coatings. Part I: a linear dielectric mixture equation, Corros. Sci. 45 (2003) 1631–1646, https://doi.org/10.1016/S0010-938X(03)00014-3.
[54] A.S. Nguyen, N. Causse, M. Musiani, M.E. Orazem, N. Pébère, B. Tribollet, V. Vivier, Determination of water uptake in organic coatings deposited on 2024 aluminium alloy: comparison between impedance measurements and gravimetry, Prog. Org. Coat. 112 (2017) 93–100, https://doi.org/10.1016/j.porgcoat.2017.07.004.
[55] A. Roggero, L. Villareal, N. Caussé, A. Santos, N. Pébère, Correlation between the physical structure of a commercially formulated epoxy paint and its electrochemical impedance response, Prog. Org. Coat. 146 (2020), 105729, https://doi.org/10.1016/j.porgcoat.2020.105729.
[56] D.M. Brasher, A.H. Kingsbury, Electrical measurements in the study of immersed paint coatings on metal. I. Comparison between capacitance and gravimetric methods of estimating water-uptake, J. Appl. Chem. 4 (1954) 62–72, https://doi.org/10.1002/jctb.5010040202.
[57] A. Roggero, N. Caussé, E. Dantras, L. Villareal, A. Santos, N. Pébère, In situ study of the temperature activated kinetics of water sorption in an epoxy varnish, Polymer (Guildf.) 213 (2021), 123206, https://doi.org/10.1016/j.polymer.2020.123206.
[58] J. Crank, The Mathematics of Diffusion, Oxford Science Publications, 1975.
[59] S.B. Lee, T.J. Rockett, R.D. Hoffman, Interactions of water with unsaturated polyester, vinyl ester and acrylic resins, Polymer (Guildf.) 33 (1992) 3691–3697, https://doi.org/10.1016/0032-3861(92)90657-I.
[60] S.S. Morye, R.P. Wool, Mechanical properties of glass/flax hybrid composites based on a novel modified soybean oil matrix material, Polym. Compos. 26 (2005) 407–416, https://doi.org/10.1002/pc.20099.
[61] N. Manthey, F. Cardona, G. Francucci, T. Aravinthan, Thermo-mechanical properties of acrylated epoxidized hemp oil based biocomposites, J. Compos. Mater. 48 (2014) 1611–1622, https://doi.org/10.1177/0021998313488155.
[62] M.E. Orazem, B. Tribollet, Electrochemical Impedance Spectroscopy, 2nd edition, John Wiley & Sons, Hoboken, New Jersey, 2017.